Issued: 26 March 1979

NASA Contractor Report 159079

Part III of Final Report

Under Contract NASI-15288

Technical Report FWA79-003

DESIGN STUDY FOR FUTURE SATELLITE MICROWAVE SCATTEROMETERS

by Frank J. Wentz

Prepared for

NASA

National Aeronautics and Space Administration

Langley Research Center
Hampton, Virginia 23665
AC 804 827-3966

Prepared by

Frank J. Wentz & Associates

HEARST BLDG., STE 1232, SAN FRANCISCO, CA 94103

TEL (415) 957-1266

ABSTRACT

We have conducted a design study of future satellite microwave scatterometers used in sensing the sea-surface wind vector. Sensors having 2, 3, and 4 fixed antennas on one side and operating in H, V and dual HV polarization modes are considered, including the Seasat Scatterometer (SASS). The performance of these sensors is simulated on a computer, and the rms sensing errors for friction velocity U_* and wind direction χ are computed. Also, the alias removal capability of the sensors is evaluated. In the noise-free simulations, the U_* and χ are estimated very accurately, with the rms sensing errors being on the average less than 0.1% and 0.2°, respectively. These small residual errors are due to numerical noise in the U_*,χ estimator. In the absence of noise, perfect alias removal is achieved for all sensors having three or four antennas and for 2-antenna sensors operating in the dual HV polarization mode, with a few noted exceptions. As expected, the 2-antenna, single polarization sensors demonstrate no alias removal capability. Going to the noise-added simulations, the dual HV polarization mode is always superior to the single polarization modes. Furthermore, these simulations clearly indicate that for the 2-antenna sensors the optimum antenna separation is 90°, which corresponds to the SASS. The SASS configuration operating in the HV mode yields rms sensing errors of 4% for U_* and 8° for χ. In the presence of noise, none of the 2-antenna sensors performed well in resolving aliases. Increasing the number of antennas to three or four greatly improves the alias removal capability. For certain antenna geometries operating in dual polarization, the highest probability alias is the correct solution about 90% of the time. The 3-antenna configuration with the overall best performance has a constant 60° separation between adjacent antennas. Similarly, the best performing 4-antenna config-

uration has a constant 40° separation between adjacent antennas. The rms sensing errors for these two configurations are about 3% for $U_{\star}$ and 5° for χ when using dual polarization. When considering possible hardward tradeoffs, one should note that the improvement in performance is not that significant when going from three antennas to four. Furthermore, there are several other 3 and 4 antenna configurations that perform nearly as well as the two mentioned above.

TABLE OF CONTENTS

SECTION 1. INTRODUCTION

The design of future satellite microwave scatterometers, used in sensing sea-surface wind vector, can be greatly enhanced by first simulating on a computer the operation of feasible sensor configurations. In view of this, we have conducted simulations for a large number of scatterometer antenna configurations and polarization modes. The Seasat Scatterometer (SASS) is included in the set of feasible sensors. The results of the simulations are expressed in terms of performance statistics. These statistics relate to the wind-direction alias removal capability and to the rms sensing errors for friction velocity U_* and wind direction χ. The statistics are analyzed, and optimum scatterometer configurations are recommended. Also, we assess the absolute accuracy of the SASS in measuring U_* and χ and its capability to resolve wind direction aliases.

SECTION 2. ANTENNA CONFIGURATIONS AND POLARIZATION MODES

The fundamental requirement for a feasible antenna configuration is that the scatterometer views the same area of the sea surface from at least two different azimuth directions. This requirement is necessary because the backscattering is dependent on both friction velocity and wind direction. Scatterometers utilizing two azimuth looks are capable of separating the velocity and direction effects [Grantham, et al, 1975]. For the purpose of this investigation, the azimuth viewing angle ϕ is defined as the angle made by the subtrack direction and the projection of the viewing vector onto the sea surface. The viewing vector points from the scatterometer to the sea surface area being observed. An observation for which $\phi = 0°$ ($\phi = 180°$) is along the subtrack in the forward (backward) direction. A sidelook making a right angle with the subtrack is indicated by $\phi = 90°$ or $270°$. We only consider fixed antennas having constant azimuth angles. Hence, for a set of antennas to view the same area of the sea surface, their azimuth angles must lie either between $0°$ and $180°$ (right-side viewing) or between $180°$ and $360°$ (left-side viewing).

The simulations are performed for two, three, and four antennas viewing the right side of the subtrack. The simulation results are, of course, equally applicable to left-side viewing. In order to have an appreciable swath width, we further require that the antenna azimuth angles be greater than or equal to $30°$ and less than or equal to $150°$. This requirement results in the maximum separation between antennas being $120°$. The minimum separation between adjacent antennas is set at $30°$. The smallest allowed azimuth angle increment going from one configuration to another is set at $15°$. These two restrictions reduce the number of possible an-

tenna configurations to a manageable level, while maintaining a representative ensemble. Figure 1 shows the 23 antenna geometries satisfying the above stated requirements and restrictions. We have also included a 24th configuration for which there are four antennas separated by 40° from each other. This configuration is included because of its overall symmetry. Each configuration is labelled by two numbers. The first number denotes the number of antennas, and the second number is used to distinguish the various geometries. For instance, Configuration 2/5 is the SASS.

For each antenna geometry, three polarization modes are considered. Mode H (V) refers to the case in which each antenna views the surface with horizontal (vertical) polarized radiation. Mode HV is a combination of Mode H and Mode V in that each antenna views the surface with both horizontal and vertical polarized radiation. Mode HV should not be confused with cross-polarization measurements, which are not considered in this investigation.

Due to the limited scope of this study, we only consider one earth incidence angle θ_i. The AAFE/RADSCAT Scatterometer Program [Jones, et al, 1977] indicated that $\theta_i = 40°$ is an ideal angle for measuring U_* and χ. At smaller θ_i the dependence of the normalized radar cross section (NRCS) on U_* is weaker, and at larger θ_i the signal to noise is poorer. In view of this, θ_i was set to 40° for all simulations.

Figure 1. Feasible Antenna Configurations

SECTION 3. SEA-SURFACE WIND STATES

In the simulations we assume that each antenna views the same sea-surface wind state characterized by a friction velocity $U_\star$ and wind direction χ. Three friction velocities, $U_\star$ = 20, 50, and 100 cm/sec, are considered and roughly correspond to wind speeds of 5, 10, and 20 m/sec. Twenty-four wind directions are considered, $\chi = 0°, 15°, \cdots, 345°$. The angles refer to the wind direction, in the out-of meteorological sense, relative to the subtrack direction. That is to say, $\chi = 0°$ and $\phi = 0°$ corresponds to an upwind observation. Thus a total of $3 \times 24 = 72$ sea-surface wind states are treated in the simulations.

SECTION 4. DESCRIPTION OF SIMULATIONS

Figure 2 is a flow diagram of the various processing steps that comprise a simulation. Firstly, one of the 24 antenna configurations shown in Figure 1 is selected along with one of the 3 polarization modes. Next, the friction velocity U_* and the wind direction χ are set. In order to consider all possible combinations of the 3 U_*'s and the 24 χ's, a nested do-loop structure is employed. The outer loop is for U_* and the inner loop is for χ.

A set of sea-surface NRCS is then computed for the specified antenna configuration/polarization mode, U_*, and χ. A model function described by Wentz [1978a] is used to compute the NRCS. The model represents a fit to the AAFE/RADSCAT NRCS measurements of the North Sea [Jones and Schroeder, 1978]. The accuracy of the fit is 0.7 dB. This set of computed NRCS corresponds to noise-free scatterometer measurements under clear sky conditions. (We do not consider the effect of atmospheric attenuation in this investigation.)

Two types of simulations are performed: noise-free and noise-added. For the noise-free case, the set of NRCS is directly passed to the program WINVEC. This program estimates U_* and χ given a group of NRCS measurements, and is identical to the Geophysical Algorithm being used at JPL to process Seasat SASS data [Wentz, 1978b]. In the noise-added simulations, a random noise component is added to each NRCS before being processed by WINVEC. The generation of this noise is described in the next section. The noise is indicative of that experienced by SASS.

WINVEC does a 5° incremented search for wind direction. This type of search produces a slight quantization error dependent on how close the

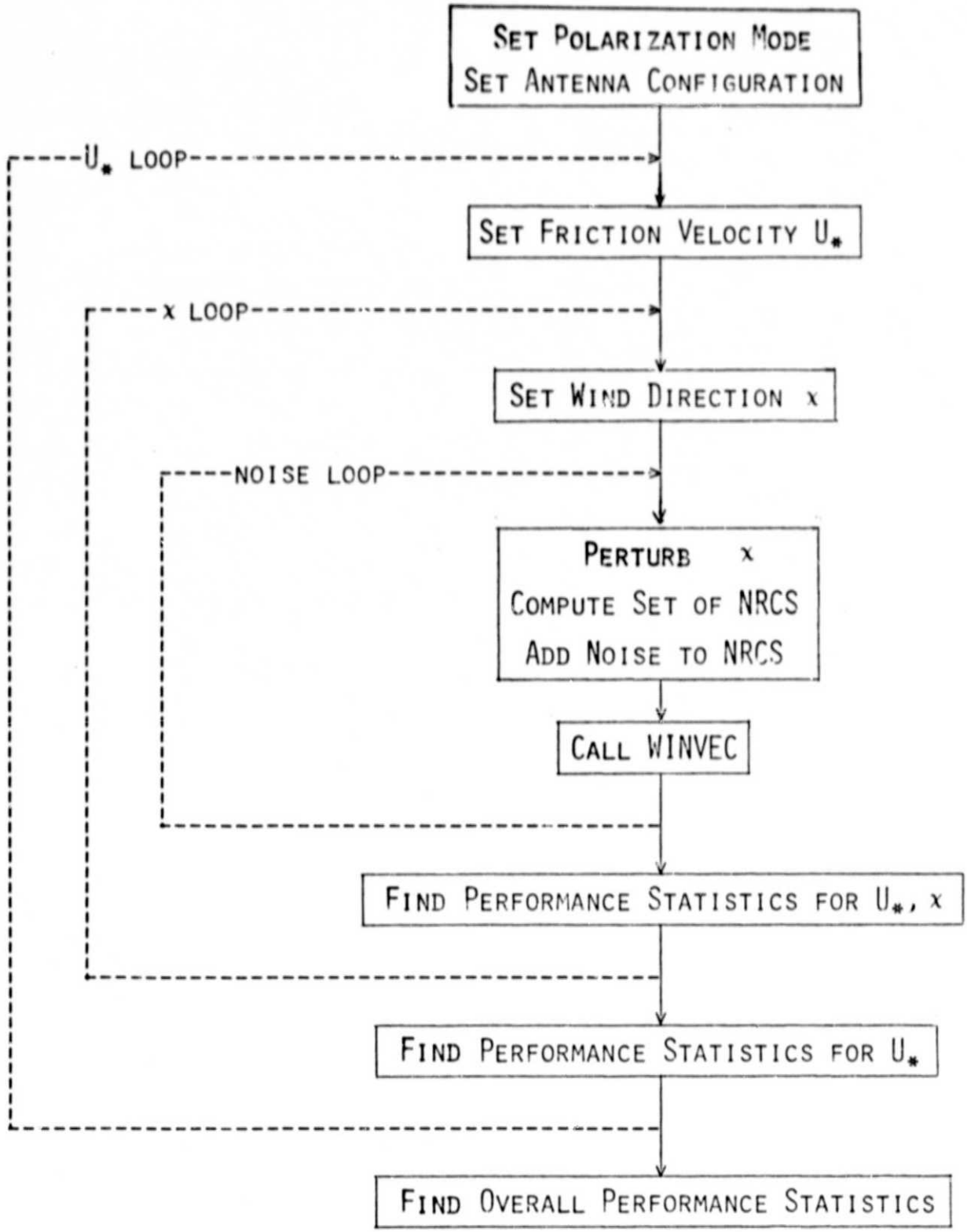

Figure 2. Flow Diagram of Simulation Program

wind direction is to a multiple of 5°. That is to say, the program's performance is somewhat better when χ is near a multiple of 5°. In order to obtain a more realistic simulation, χ is perturbed from its incremental values of 0°, 15°, ···, 345°. This perturbation is accomplished by generating a random variable having a uniform distribution on the interval -7.5° to 7.5°. This random variable is then added to the incremental value of χ. Thus the perturbed χ will lie within a ±7.5° bin centered on the incremental value.

Because of the well-known aliasing problem, WINVEC always finds two or more pairs of possible U_* and χ for each simulated measurement set. In order to compute performance statistics, the simulation program selects the pair for which the absolute difference between the estimated χ and the actual χ is a minimum. For this pair, the differences $\Delta U_* = \hat{U}_* - U_*$ and $\Delta\chi = \hat{\chi} - \chi$ are calculated, where $\hat{U}_*$ and $\hat{\chi}$ denote the estimates. Furthermore, WINVEC computes a relative probability for each U_*, χ pair. Five counters are employed to evaluate the usefulness of this relative probability. When the selected pair corresponds to the pair having the highest (second highest, ···, fifth highest or less) probability, the N_1 (N_2, ···, N_5) counter is incremented by one.

Various ensembles of simulated measurement sets are generated by the U_* and χ loops and by the noise loop described in the next paragraph. From these ensembles performance statistics are computed. These statistics consist of the mean friction velocity and wind direction errors, $\langle\Delta U_*\rangle$ and $\langle\Delta\chi\rangle$, and the rms friction velocity and wind direction errors, $\langle\Delta U_*^2\rangle^{\frac{1}{2}}$ and $\langle\Delta\chi^2\rangle^{\frac{1}{2}}$. Also, the percentage of time P_1 (P_2, ···, P_5) that the highest (second highest, ···, fifth highest or less) probability alias corresponded to the correct solution is computed. The expressions for calculating these sta-

tistics are as follows:

$$\langle \Delta U_\star \rangle = (1/I) \sum_{i=1}^{I} (\Delta U_\star)_i \tag{1}$$

$$\langle \Delta \chi \rangle = (1/I) \sum_{i=1}^{I} (\Delta \chi)_i \tag{2}$$

$$\langle \Delta U_\star^2 \rangle = (1/I) \sum_{i=1}^{I} (\Delta U_\star^2)_i \tag{3}$$

$$\langle \Delta \chi^2 \rangle = (1/I) \sum_{i=1}^{I} (\Delta \chi^2)_i \tag{4}$$

$$P_j = N_j \Big/ \sum_{j=1}^{5} N_j \tag{5}$$

where I is the number of measurement sets in the given ensemble.

When noise is added, an additional inner-most loop, shown in Figure 2, is required to ensure statistically significant results for a given $U_\star$ and χ. The loop is performed 25 times. In each loop, χ is perturbed a different amount within the ±7.5° bin, and new noise components are added to the computed NRCS. After completion of the inner-most noise loop, the performance statistics are computed for the ensemble of 25 individual sets of measurements. These statistics are indicative of the performance of the considered antenna configuration/polarization mode when viewing a wind state corresponding to the specified $U_\star$ and χ.

At the completion of the χ loop, the results of the 24 wind directions are averaged together, thereby determining the performance statistics for the specified $U_\star$, independent of χ. Finally, when the outer $U_\star$ loop is finished, overall performance statistics are computed for the selected antenna configuration/polarization mode, independent of $U_\star$ and χ. The analyses presented in the following sections are based on these overall statistics.

SECTION 5. SIMULATED NOISE

In the noise-added simulations, a random noise component is added to each NRCS in the set before being processed by WINVEC. The noise, expressed in terms of decibels, is assumed to be normally distributed, having a zero mean and a standard deviation $\Delta\sigma_o$. The noise figures for the SASS are used to specify $\Delta\sigma_o$ in the simulation. The SASS expressions for $\Delta\sigma_o$ are [Schroeder, 1978]:

$$\Delta\sigma_o = 10 \log e \left[\Delta_a^2 + \Delta_s^2 + \Delta_b^2 + K_p^2 \right]^{\frac{1}{2}} \tag{6}$$

where $\log e = 0.4342\cdots$ and the three Δ's denote percent errors due to attitude, system, and absolute calibration, respectively. For $\theta_i = 40°$, their values are 3%, 2%, and 12%, respectively. The remaining term K_p is due to the receiver communication noise and is given by [E. M. Bracalente, private communication, 1978]:

$$K_p^2 = (1 + 2N + AN^2)/B_c T_s \tag{7}$$

$$A = (1 + T_g/T_n)(T_g/T_s) \tag{8}$$

where N is the noise to signal power ratio and B_c is the SASS doppler bandwidth. For $\theta_i = 40°$, we use a value of 13726 Hz for B_c, which corresponds to SASS Cell 5 [Grantham, et al, 1975]. The times T_s, T_n, and T_g are the signal integration period, the noise integration period, and the range gate period. Their values are 0.2928, 0.4818, and 0.5175 sec, respectively. For a given observation geometry, the signal power is proportional to the NRCS. Hence, the signal to noise ratio, i.e., 1/N, can be expressed in terms of σ_o, the NRCS in decibels.

$$1/N = C\ 10^{\sigma_o / 10} \tag{9}$$

The proportionality constant C is found to be approximately 47 using the values appearing in Tables I and II in Schroeder [1978].

In summary, the sea-surface NRCS, denoted by σ_o, is calculated by the model function. This NRCS is then substituted into (9) which calculates the signal to noise ratio. Eqs. (6) through (8) then find the NRCS standard deviation $\Delta\sigma_o$, given the signal to noise ratio. A Gaussian random number generator is called and outputs a random variable having zero mean and unit standard deviation. The random variable is multiplied by $\Delta\sigma_o$, and the result is added to σ_o, thereby obtaining a simulated noisy NRCS.

SECTION 6. RESULTS FOR NOISE-FREE SIMULATIONS

In the noise-free simulations, the estimates of U_* and χ for the correctly selected alias should, in theory, exactly equal the specified values. That is to say, ΔU_* and $\Delta\chi$ should always be zero. Furthermore, perfect alias removal capability should be achieved by all sensors having 3 or 4 antennas and by 2 antenna sensors operating in the HV polarization mode. By perfect alias removal capability, we mean that the alias with the highest probability is always the correct solution, i.e., $P_1 = 100\%$; P_2, P_3, P_4, and $P_5 = 0$. These assertions concerning ΔU_*, $\Delta\chi$, and alias removal are based on the following fact. In the absence of noise, the problem of recovering U_* and χ reduces to solving a set of transcendental equations. The equations correspond to the NRCS model function set equal to the various simulated measurements. For 2 antennas and single polarization, multiple point solutions exist. For all other configurations, a single point solution exists.

Although no noise is added to the NRCS, there is some noise inherent in the program WINVEC. This noise is, in a large part, due to the 5° incremental search for wind direction discussed in Section 4. Also, some error results from limited precision arithmetic. This numerical noise prohibits the exact recovery of U_* and χ and resolving of aliases. However, the numerical noise is much less than the instrumental noise described in Section 5, and near-perfect results are indeed obtained from the simulations. The noise-free rms errors $\langle \Delta U_*^2 \rangle^{\frac{1}{2}}$ and $\langle \Delta\chi^2 \rangle^{\frac{1}{2}}$ are on the average less than 0.1% and 0.2°, respectively. Furthermore, WINVEC clearly demonstrated its capability in the absence of noise to remove aliases. For all sensors operating in the HV polarization mode, the highest probability alias always corresponds to the correct solution, i.e., $P_1 = 100\%$. All of the 3 and 4-antenna sensors also have $P_1 = 100\%$, with a few exceptions. These excep-

tions are for V polarization observations of a $U_\star$ = 50 cm/sec wind state. For these cases, P_1 is about 90%, P_2 is about 10%, and P_3, P_4, and P_5 are 0%. The explanation for the exceptions is that the upwind and downwind NRCS for vertical polarization and $U_\star$ = 50 cm/sec are nearly equal. If there were perfect upwind/downwind symmetry, then two unresolvable aliases would always exist, regardless of antenna configuration and polarization mode. Finally, as expected, the 2-antenna, single polarization sensors demonstrate no alias removal capability.

SECTION 7. RESULTS FOR NOISE-ADDED SIMULATIONS

Tables 1, 2, and 3 give the performance statistics for a sensor operating in the H, V, and HV polarization modes, respectively. Each table is vertically grouped according to the number of antennas. The statistics are for the noise-added case and consist of the rms sensing errors for friction velocity and wind direction, $\langle \Delta U_*^2 \rangle^{\frac{1}{2}}$ and $\langle \Delta \chi^2 \rangle^{\frac{1}{2}}$. Also included in the tables are the percentage of time P_1 (P_2, $\cdots$, P_5) that the highest (second highest, $\cdots$, fifth highest or less) probability alias is the correct solution. The mean sensing errors, $\langle \Delta U_* \rangle$ and $\langle \Delta \chi \rangle$, which are not in the tables, are generally about 0.1% and 0.1°, respectively. These small values indicate that the estimation is essentially unbiased.

In analyzing the two-antenna sensors, we see that the optimum separation between antennas is 90°, which corresponds to the SASS configuration. This is clearly shown in Figures 3 and 4, where the U_* and χ rms errors are plotted versus the antenna separation angle. Each figure contains three curves corresponding to the three polarization modes. In all cases, the sensing error reaches a minimum near 90°. The H polarization mode has the largest error because of the poor signal to noise that occurs for this polarization. On the other hand, the HV mode has the smallest error because in this mode four measurements are taken as compared to two measurements for the single polarization modes. Thus, the minimum rms sensing errors for two antennas occur for an antenna separation of 90° and an HV polarization mode. These minimum errors are about 4% for U_* and 8° for χ.

The single polarization, two-antenna sensors have poor alias removal capabilities as is indicated by P_1 being about 35% to 40%. The dual polarization, two-antenna sensors perform better in alias removal, having a P_1 of about 55%. Hence, for the HV mode, the highest probability alias is the

Table 1. Performance Statistics for H Pol Mode

Antenna Configuration (see Figure 1)	$\langle \Delta U_* ^2 \rangle^{\frac{1}{2}}$ (%)	$\langle \Delta \chi^2 \rangle^{\frac{1}{2}}$ (degrees)	P_1 (%)	P_2 (%)	P_3 (%)	P_4 (%)	P_5 (%)
2/1	10.4	20.5	39.1	29.4	17.8	12.6	1.2
2/2	9.0	19.1	38.0	28.6	19.6	12.8	1.1
2/3	8.1	17.4	40.9	26.7	19.0	13.3	.1
2/4	8.1	16.5	40.8	25.0	21.1	13.1	0.
2/5 (SASS)	7.8	15.4	38.1	25.6	23.5	12.8	0.
2/6	8.3	14.9	37.6	28.0	22.0	12.4	0.
2/7	8.5	15.5	39.2	27.2	22.6	11.0	0.
3/1	8.1	18.5	53.1	33.7	10.4	2.8	0.
3/2	7.1	17.3	57.4	34.1	7.1	1.3	0.
3/3	6.4	15.9	61.7	31.1	6.2	1.1	0.
3/4	6.4	14.7	63.1	31.7	4.6	.6	.1
3/5	6.7	14.0	63.8	30.3	5.3	.6	0.
3/6	6.2	15.5	63.6	31.4	4.6	.3	0.
3/7	6.0	14.6	67.1	28.6	4.0	.2	.1
3/8	6.4	13.6	66.3	29.8	3.8	.2	0.
3/9	6.2	12.6	67.3	29.3	3.4	0.	0.
4/1	6.0	15.3	65.0	31.3	3.4	.3	0.
4/2	5.5	12.8	68.6	29.0	2.4	0.	0.
4/3	5.5	12.7	70.8	26.9	2.3	0.	0.
4/4	5.5	14.1	68.8	28.9	2.3	0.	0.
4/5	5.8	13.3	70.7	26.7	2.5	.2	0.
4/6	5.3	12.7	72.0	26.4	1.6	0.	0.
4/7	5.5	13.0	71.9	26.1	1.8	.1	0.
4/8	5.3	13.0	72.1	26.2	1.7	0.	0.

Table 2. Performance Statistics for V Pol Mode

Antenna Configuration (see Figure 1)	$\langle \Delta U_* ^2 \rangle^{\frac{1}{2}}$ (%)	$\langle \Delta \chi^2 \rangle^{\frac{1}{2}}$ (degrees)	P_1 (%)	P_2 (%)	P_3 (%)	P_4 (%)	P_5 (%)
2/1	9.9	15.5	37.2	32.1	16.1	14.7	0.
2/2	7.8	12.2	34.7	30.9	17.4	16.9	0.
2/3	6.2	10.0	35.3	29.3	20.4	14.9	0.
2/4	5.8	9.1	35.8	26.8	21.2	16.1	0.
2/5 (SASS)	5.3	9.0	34.2	26.2	23.0	16.6	0.
2/6	5.8	9.5	34.7	27.7	21.1	16.6	0.
2/7	6.4	10.0	36.2	27.3	21.8	14.7	0.
3/1	7.1	11.5	51.1	39.4	6.6	2.9	0.
3/2	5.8	9.8	56.6	38.1	3.4	1.9	0.
3/3	4.6	9.0	57.9	39.1	2.3	.7	0.
3/4	4.6	8.7	60.1	38.4	1.2	.3	.1
3/5	4.8	8.8	59.3	37.8	2.2	.7	0.
3/6	4.6	8.5	62.9	36.2	.6	.3	0.
3/7	4.4	7.8	64.2	35.3	.2	.3	0.
3/8	4.4	7.7	64.0	35.6	.3	.1	0.
3/9	4.4	7.6	64.3	35.7	.1	0.	0.
4/1	4.4	7.9	63.2	36.2	.5	.1	0.
4/2	3.9	6.6	66.2	33.7	.1	0.	0.
4/3	3.9	6.6	66.9	33.1	.1	0.	0.
4/4	3.9	7.2	64.9	34.7	.4	0.	0.
4/5	3.9	6.8	66.9	33.0	.1	0.	0.
4/6	3.7	6.8	65.7	34.2	.1	0.	0.
4/7	3.7	6.7	66.6	33.4	0.	0.	0.
4/8	3.7	6.4	68.9	31.1	.1	0.	0.

Table 3. Performance Statistics for HV Pol Mode

Antenna Configuration (see Figure 1)	$\langle \Delta U_*^2 \rangle^{\frac{1}{2}}$ (%)	$\langle \Delta \chi^2 \rangle^{\frac{1}{2}}$ (degrees)	P_1 (%)	P_2 (%)	P_3 (%)	P_4 (%)	P_5 (%)
2/1	9.2	14.8	56.8	25.8	12.6	4.4	.3
2/2	6.7	11.4	55.9	25.5	13.7	4.9	0.
2/3	5.1	9.4	55.9	24.7	13.5	5.9	0.
2/4	4.4	8.2	53.6	26.6	12.6	7.2	0.
2/5 (SASS)	4.1	7.9	51.4	29.2	12.8	6.6	0.
2/6	4.4	8.0	53.1	28.2	12.7	6.1	0.
2/7	5.5	9.6	58.3	25.4	11.4	4.8	0.
3/1	5.1	9.3	75.8	20.4	3.1	.6	0.
3/2	4.4	8.2	80.0	18.8	1.1	.2	0.
3/3	3.7	7.0	82.7	16.8	.4	.1	0.
3/4	3.5	6.8	82.9	16.6	.4	0.	0.
3/5	3.7	6.5	84.6	14.6	.8	.1	0.
3/6	3.9	7.2	84.4	15.2	.3	0.	0.
3/7	3.5	6.3	85.9	13.9	.2	0.	0.
3/8	3.5	6.0	87.7	12.2	.1	0.	0.
3/9	3.2	5.8	85.9	13.9	.2	0.	0.
4/1	3.5	6.3	86.6	13.2	.2	0.	.1
4/2	3.2	5.4	88.6	11.4	0.	0.	0.
4/3	3.0	5.3	90.1	9.9	0.	0.	0.
4/4	3.0	5.5	89.3	10.6	.1	0.	0.
4/5	2.8	5.1	91.1	8.9	.1	0.	0.
4/6	3.0	5.4	89.3	10.7	.1	0.	0.
4/7	3.0	5.2	90.3	9.7	.1	0.	0.
4/8	3.0	5.0	90.3	9.7	0.	0.	0.

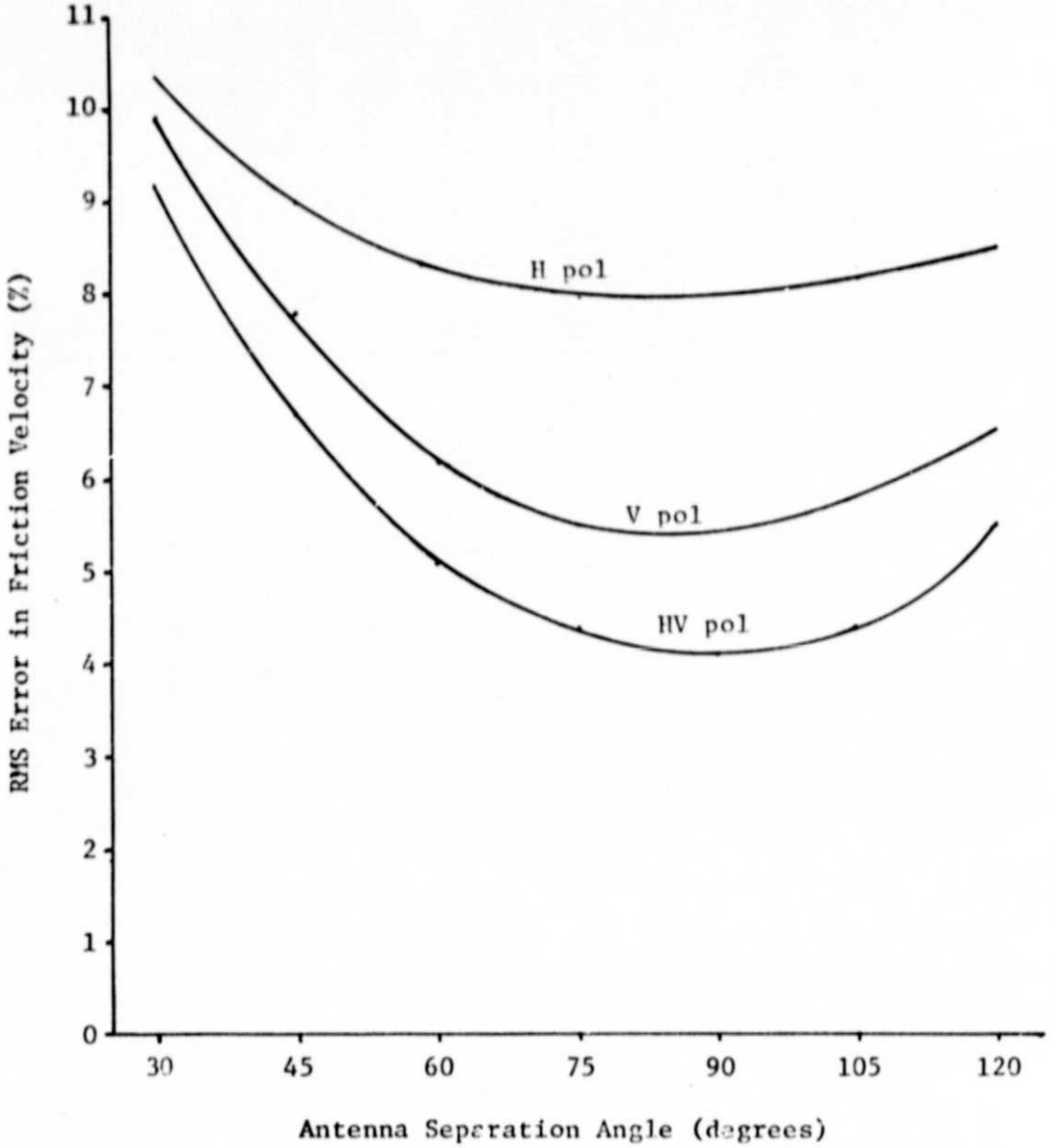

Figure 3. RMS Sensing Error in Friction Velocity Versus Separation Angle Between Two Antennas

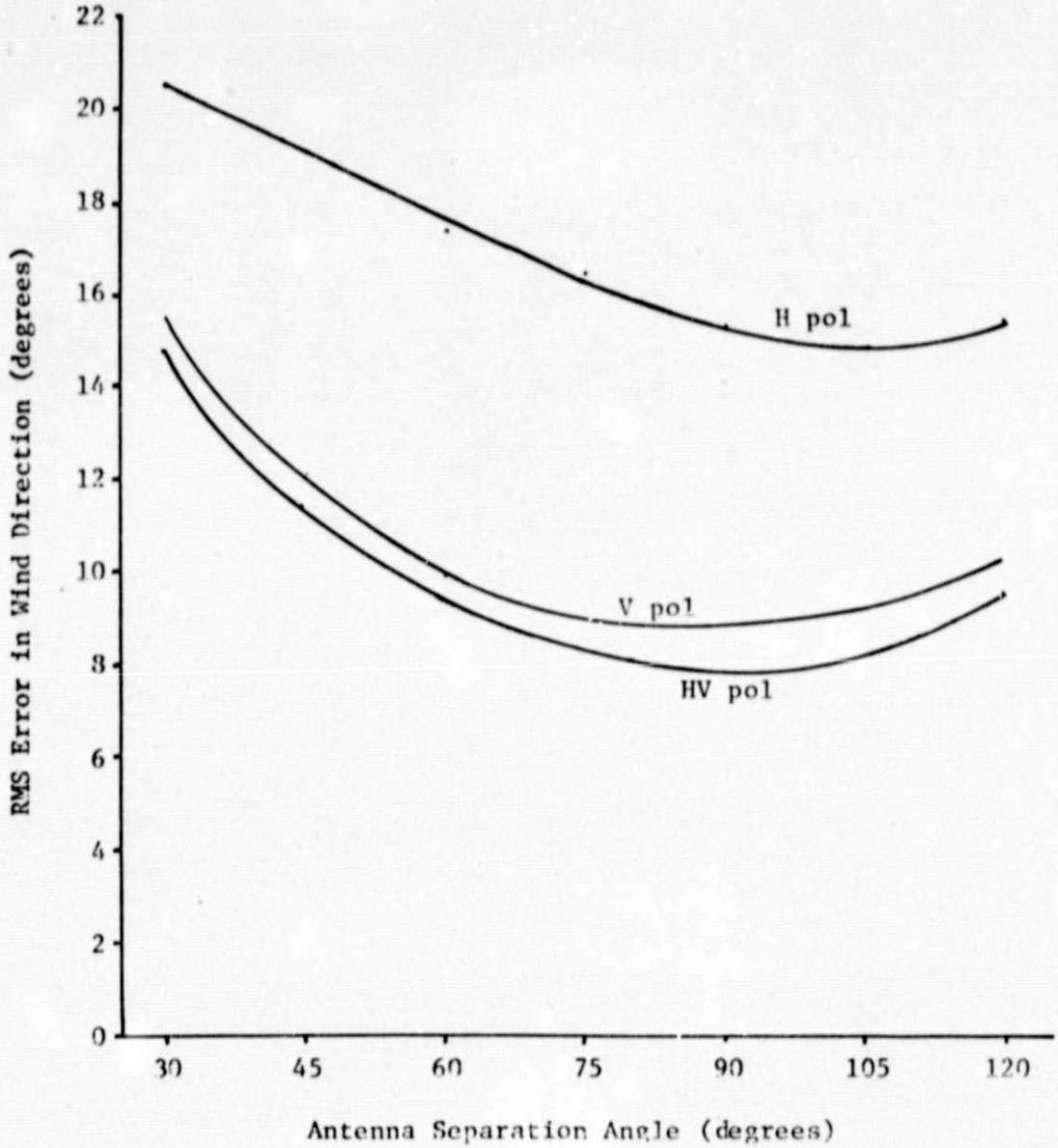

Figure 4. RMS Sensing Error in Wind Direction Versus Separation Angle Between Two Antennas

correct solution about half of the time. We also note that P_1 is relatively insensitive to antenna separation.

The alias removal capability is considerably better for three and four tennas, with P_1 reaching a maximum value of about 90% for dual polarization. Also, the U_* and χ rms sensing errors are less for three and four antennas. The reduction in sensing errors is due to the larger number of measurements. For instance, a four antenna configuration represents twice as many measurements as a two antenna configuration. Hence, the rms errors should be reduced approximately by a factor of $\sqrt{2}$. The performance tables show that this is the case. With respect to sensing errors and alias removal capability, the antenna configurations with the overall best performance are 3/9 for 3 antennas and 4/8 for 4 antennas. These configurations, as shown in Figure 1, have the maximum allowable separation of 120° between the first and last antennas and have constant spacing between adjacent antennas. We also note that the improvement in performance is not that marked when going from three antennas to four. Furthermore, there are several other three and four antenna configurations that perform nearly as well as configurations 3/9 and 4/8.

SECTION 8. CONCLUSIONS

We have conducted performance simulations for a large number of feasible scatterometer configurations and polarization modes. In particular, sensors having 2, 3, and 4 fixed antennas on one side and operating in H, V, and dual HV polarization modes are considered, including the Seasat Scatterometer (SASS). Both noise-free and noise-add simulations are performed. The generated noise is indicative of that experienced by SASS.

In the noise-free simulations, WINVEC, the current SASS Geophysical Processor, computes very accurate estimates of friction velocity U_* and wind direction χ and is able to remove aliases. In the absence of noise, the rms sensing errors for U_* and χ are on the average less than 0.1% and 0.2°, respectively. These small residual errors are indicative of the numerical noise inherent in WINVEC. Furthermore, perfect alias removal is achieved for all sensors having three or four antennas and for 2-antenna sensors operating in the dual HV polarization mode, with a few noted exceptions. By perfect alias removal, we mean that the alias with the highest probability is always the correct solution. Also, as expected, the 2-antenna, single polarization sensors demonstrate no alias removal capability.

The noise-added simulations provide a realistic assessment of the relative performance of the considered sensors. For all sensor geometries, the dual HV polarization mode is superior to the single polarization modes. The reason for this superiority is twofold. Firstly, twice as many measurements are taken in the dual polarization mode, as compared to the single polarization mode. Secondly, a dual polarization measurement represents two independent and unique pieces of information because the NRCS for H and V polarization have quite different microwave signatures. This uniqueness in

polarization is particularly helpful in removing aliases.

For 2-antenna sensors, the rms sensing errors reach a minimum when the antenna separation angle is near 90°. Hence, the SASS configuration represents the optimum geometry for 2-antenna sensors. These minimum rms errors for the dual HV polarization mode are 4% for U_* and 8° for χ. With respect to alias removal, the single polarization, 2-antenna sensors perform poorly, with the highest probability alias being the correct solution only about 35% to 40% of the time. Going to dual HV polarization increases this percentage to about 55%.

The alias removal capability is considerably better for three and four antennas, with the highest probability alias being correct about 90% of the time for certain antenna geometries operating in the dual polarization mode. The 3-antenna configuration with the overall best performance has a constant 60° separation between adjacent antennas. Similarly, the best performing 4-antenna configuration has a constant 40° separation between adjacent antennas. The rms sensing errors for these two configurations are about 3% for U_* and 5° for χ when using dual polarization. When considering possible hardward tradeoffs, one should note that the improvement in performance is not that significant when going from three antennas to four. Furthermore, there are several other 3 and 4 antenna configurations that perform nearly as well as the two mentioned above.

SECTION 9. REFERENCES

Grantham, W., E. Bracalente, W. Jones, J. Schrader, L. Schroeder, J. Mitchell, "An Operational Satellite Scatterometer for Wind Vector Measurements Over the Ocean," NASA TM X-72672, March 1975.

Jones, W. L., L. C. Schroeder, and J. L. Mitchell, "Aircraft Measurements of the Mircowave Scattering Signature of the Ocean," IEEE Oceanic Engineering 2 (1), pp. 52-61, January 1977.

Jones, W. L., and L. C. Schroeder, "Radar Backscatter From the Ocean: Dependence on Surface Friction Velocity," Boundary-Layer Meteorology, Volume 13, pp. 133-149, January 1978.

Schroeder, L. C., "Seasat-A Satellite Scatterometer (SASS) Validation and Experiment Plan," NASA TM X-78751, May 1978.

Wentz, F. J., "Estimation of the Sea Surface's Two-Scale Backscatter Parameters," NASA Contractor Report 145255, March 1978a.

Wentz, F. J., "Documentation for Program WINVEC: Computation of Statistics on the Sea-Surface Friction Velocity and Wind Direction," Wentz Associates Technical Report 78-001, January 1978b.